Magnetostructural Transition Kinetics in Shocked Iron

Michael P. Surh,* Lorin X. Benedict,† and Babak Sadigh‡
Lawrence Livermore National Laboratory, Livermore, California 94550, USA
(Received 19 April 2016; revised manuscript received 21 June 2016; published 15 August 2016)

A generalized Heisenberg model is implemented to study the effect of thermal magnetic disorder on kinetics of the Fe $\alpha-\epsilon$ transition. The barrier to bulk martensitic displacement remains large in α-Fe shocked well past the phase line but is much reduced in the [001] α-ϵ boundary. The first result is consistent with observed overdriving to metastable α, while the second suggests structural instability, as implied by observation of a [001] shock transformation front without plastic relaxation. Reconciling both behaviors may require concurrent treatment of magnetic and structural order.

DOI: 10.1103/PhysRevLett.117.085701

Recently developed, *in situ* x-ray studies of shock compression can probe the nonequilibrium time evolution of phase transitions, besides locating them within the equilibrium phase diagram. The archetypal system of elemental Fe transforms near 13 GPa pressure from the ferromagnetic (FM) bcc α to the hcp ϵ phase [1,2], where ϵ is antiferromagnetic (AFM) [3] or has fluctuating local moments [4,5]. Quasistatic experiments show the atomic and magnetic changes to be interrelated [6–8]. Fast (2–6 ns) [001]-oriented shocks of single crystal α find that threshold 6% compression at 13 GPa drives a transition to an ϵ-like phase with volume collapse to 15%–18% [001] compression [9]. Remarkably, the transition is practically reversible—no plastic wave is seen despite high elastic strain in both phases [10], and recovered samples largely retain single crystal character [9–11]. This unusual behavior has been attributed to unstable (barrier-free) martensitic displacement. Molecular dynamics simulations (MD) exhibiting no martensitic barrier predicted this [12], forming a transformation front in just 1–2 ps near threshold shock compression. However, the interatomic potential depends only implicitly on magnetic order. In contrast, ultrafast (270 ps) shock experiments overdrive polycrystalline samples substantially (20–25 GPa) without transformation [13], suggesting a significant activation barrier to nucleation of a first order transition. The different experimental kinetics may relate to differences in magnetic order between bulk and the α-ϵ interface, in which case a single, nonmagnetic interatomic potential might not capture the full range of behavior.

In the present work, we use density functional theory (DFT) and model calculations to show that the barrier to bulk α-ϵ martensitic displacement persists to >8% [001] uniaxial strain, even with thermal magnetic disorder. Thus, shocks may compress Fe beyond the equilibrium phase line into metastability. At the same time, magnetic frustration is enhanced in the boundary between competing phases, and we suggest that the martensitic barrier may vanish within the [001] α-ϵ shock front closer to threshold compressions. Once ϵ nuclei form (probably heterogeneously) and grow into a shock transformation front, atoms at the [001] interface may undergo martensitic displacement along with changes in magnetic order and layer spacing, collapsing layer by layer. The shock front subsequently propagates without thermal activation or plastic accommodation.

Ground state DFT calculations predict a significant α-ϵ structural transition barrier under *hydrostatic* pressure [3,14–16]; [001] compression is similar. Figure 1 shows total energies of Fe for two [001] *uniaxial* compressions versus the bulk martensitic shuffle displacement δ, corresponding to a T_1 N-point phonon, shifting alternate (110) bcc atomic planes in opposite $[1\bar{1}0]$ directions. The bulk martensitic barrier, labeled ΔE_M in Fig. 1, is >45 meV/atom near the experimental threshold

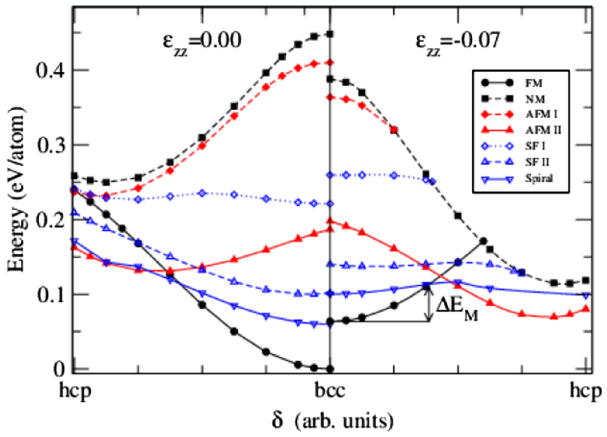

FIG. 1. Total energies of Fe magnetic phases at [001] compressions of 0%, 7% (left, right) are shown versus amplitude of the martensitic shuffle displacement, δ [14], from bcc at center to hcp at the ends. Spin states include ferromagnetic (FM), nonmagnetic (NM), two-site collinear antiferromagnetic phases (AFM), corresponding "spin-flop" (SF) structures midway between these AFM and the FM phases, and a low-energy spin-spiral structure. The hcp-like ground state Ref. [3], is AFM (local moments $\geq$ 0.5 Bohr magneton).

compression [17]. Energies are obtained by VASP GGA-PAW with EMAX $\simeq$ 300 eV [18–21] and 8000 k points for 4 atom unit cells. Magnetic phases considered here include both constrained and unconstrained spin structures of up to 16 atoms [22]. For reference, the equilibrium lattice constant of 2.824 Å is underestimated versus experiment (2.87 Å [25]), and elastic moduli are overestimated by 25% with this method. (The unshocked state in these calculations is taken at the equilibrium DFT lattice constant rather than the experimental value).

The broad energy dispersions in Fig. 1 imply strong magnon-phonon coupling. This causes Fe structural properties to vary with temperature and thermal spin disorder; e.g., phonon softening anomalies are prominent near the Curie temperature [26,27]. Magnetic frustration is evident as many phases approach degeneracy near the transition state, suggesting that spin entropy might lower the martensitic free energy barrier, too. A prior study of the α-ϵ transition under hydrostatic stress included magnetic disorder, fitting a Heisenberg model to disordered local moment (DLM) calculations with collinear spin; however, it predicted a nonzero barrier for the martensitic transition path (albeit for *hydrostatic* pressure) [28]. Such magneto-structural coupling may also influence shock behavior. In particular, Fig. 1 sets an overall energy scale, $\Delta E_{\text{FM-AFM}}$, which decreases versus ϵ_{zz} and δ. The Curie temperature scales with this, so [001] shocks could conceivably disorder local magnetic moments even without heating the material excessively. Figure 1 then suggests that loss of short-range FM order can destabilize bcc.

We employ a generalized Heisenberg model [29,30] fit to ordered, collinear and noncollinear spin structures to study the bulk shuffle barrier. Self-consistent DFT total energies and local moments are fit in tandem. Our model Hamiltonian is

$$H(\{\vec{\mu}\}) = E^{\text{NM}} + \sum_i \sum_{n=1}^{4} I_i^{[n]} |\vec{\mu}_i|^{2n} + \sum_{ij} \vec{\mu}_i \cdot \vec{\mu}_j (J_{ij} + K_{ij} |\vec{\mu}_i| |\vec{\mu}_j| + L_{ij} \vec{\mu}_i \cdot \vec{\mu}_j). \quad (1)$$

The energy zero is set by the $|\mu| = 0$, nonmagnetic (NM) phase. Onsite terms $I_i^{[n]}$ parametrize a spontaneous $\mu > 0$ and a susceptibility, needed because self-consistent moments vary in magnitude between FM and AFM configurations. J_{ij} represents a conventional Heisenberg coupling, approximating RKKY interactions with five nearest cubic neighbor shells, j. K_{ij}, and (biquadratic) L_{ij} terms are partial, quartic extensions of the onsite terms to the same five neighbor shells. They endow the self-consistent μ with dependence on magnetic order, as might be expected from $\vec{k}$-dependent Fermi surface nesting, and they meaningfully improve the quality of fit. A more complete set of symmetry-allowed coefficients [29,30] is not considered.

All coefficients in Eq. (1) are expanded in Taylor series of both ϵ_{zz} and δ up to second order. The DFT data include seven equispaced compressions from 0% to 12%; the fit has a total rms error of less than 3 and 5 meV/atom for cubic and tetragonal energies per atom, respectively, and 0.05 μ_B for moments (see Supplemental Material [22]). The model can be applied to cubic iron; e.g., the Curie temperature is predicted to be 1070 K, versus the experimental 1043 K, and the local moment is 2.17 μ_B versus the experimental value 2.22 μ_B [31]. However, the fitted FM energy is too high by 6 meV/atom at the highest compressions (versus DFT), and the model predicts a bcc-like AFM ground state at 9% [001] compression, contrary to DFT.

Similar fits of Eq. (1) are made to the calculated DFT uniaxial and biaxial stresses, σ_{zz} and $(\sigma_{xx} + \sigma_{yy})/2$, for $\delta = 0$. The rms error for cubic stresses is $\delta\sigma < 3$ kbar; for tetragonal cases $\delta\sigma < 8$ kbar, or about 1% of the total range of values. All stresses are then reduced by 25% of the ground state value for the given ϵ_{zz} to compensate for the overly stiff moduli predicted by DFT.

We use the model of Eq. (1) to study the bcc-like final state of planar 1D shocks, with both compression and heating. The interplay between thermally disordered local moments and atomic shuffle displacement is treated using classical Metropolis Monte Carlo simulations [32] of the generalized Heisenberg spin model for $N = 432$ atoms. The shock temperature is estimated from an equation of state [33] extended to the metastable α phase. For example, a shock starting from room temperature is estimated to reach $T = 341$ K at 6% compression. This Hugoniot assumes plastic relaxation to hydrostatic pressure, so the purely elastic, uniaxial compression that is assumed here will achieve slightly lower temperatures. Thermal magnetic disorder has a significant effect on the uniaxial stress. The $T = 0$ DFT stress at $\epsilon_{zz} = -0.06$ is 16.7 GPa (including the 25% ground state correction, while the (DFT-corrected) finite-T stress model gives $\sigma_{zz} = 14.7$ GPa at $T = 341$ K, the expected shock temperature starting from room temperature. The experimental value is $\sigma_{zz} \simeq 11.5$ GPa at 5.5%–6% [001] compression [9,10] or 12.5 GPa at 6% [13]. Predictions beyond 6% compression can be compared to (metastable) shock data in Ref. [13]: $\sigma_{zz} \simeq 17.5$ GPa at 8% versus the corrected Heisenberg model ($T = 362$ K, $\sigma_{zz} = 19.6$ GPa); and $\sigma_{zz} \simeq 22.5$ GPa at 10% versus the model ($T = 390$ K, $\sigma_{zz} = 22.9$ GPa). If these predicted shock temperatures were higher by 20 K, the stresses would be reduced to 14.5, 19.3, and 22.6 GPa at 6%, 8%, and 10%, respectively. (Note that thermal phonon contributions are not included here.)

The model predicts that AFM phases are energetically favored by [001] compression. The {111} nearest neighbor Heisenberg interaction is FM; this term dominates but decreases in strength under [001] compressions. The

next-nearest, [001]-neighbor interaction is AFM. That neighbor distance decreases rapidly under compression, and the coupling strength rises, becoming comparable in magnitude to the nearest neighbor interaction at 4% compression. Thus, T_C is predicted to drop with compression.

The martensitic barrier is expected to vanish as the T_1 shuffle mode becomes unstable. An estimate is obtained from $\omega^2 \propto \partial^2\langle H\rangle/\partial\delta^2|_{\delta=0}$, by fitting Eq. (1) to DFT energies at $\delta = 0, 1/8, 1/4$ from bcc to (nonideal) hcp. This is analogous to computing a self-consistent phonon in the presence of thermal magnetic disorder. It is also in the spirit of an interatomic potential, in which thermal electronic degrees of freedom are traced over, imposing adiabatic separation of the phonon and the (only slightly faster) magnon degrees of freedom.

The number of magnetic configurations in the equilibrium ensemble that are structurally unstable to shuffle ($\omega^2 \leq 0$) is recorded during simulations of a periodic 432-spin system. Temperature and compression both promote instability. No unstable configurations (out of $>10^5$ samples) are found at 6% compression on the shock Hugoniot of Fe from room temperature. At 8% shock compression $T = 362$ K and $\sigma_{zz} = 20$ GPa, approximately 1 in 10^5 states are unstable to shuffle displacement. At 10%, 390 K, and 23 GPa, fully 8% of all spin configurations are structurally unstable. According to classical nucleation theory in a large simulation volume, it becomes exponentially easier with temperature to achieve a critical nucleus unstable to ϵ. The appearance of an experimental structural transition in ultrafast shocks at 20–25 GPa [13] is consistent with the predicted trend.

The predicted reductions in T_C and structural stability may be slightly overestimated for two reasons, but the trend is robust. First, the model Hamiltonian slightly favors AFM relative to FM at high strain (compared to DFT). Second, the GGA-DFT energies themselves only approximate the true many-body value. The intrinsic uncertainty is seen if the unshocked state is taken at the experimental lattice constant instead of the DFT equilibrium value used here. In that case, the relative energy of the [001]-compressed FM state is reduced, and the ground state remains FM beyond 12% compression. Yet, correcting for both effects would favor increased FM stability, higher T_C, and a higher martensitic transition state barrier. Thus, all indications are that the bulk transition barrier remains substantial at 6% [001] compression and that the initial stages of α-ϵ transformation at threshold compression will follow conventional nucleation and growth kinetics for a first-order phase transition.

The analysis so far has been limited to bulk martensitic transitions, as may occur in homogeneous nucleation. DFT calculations are also made for a small, simplified model of the [001] α-ϵ interface, in a periodic 24-atom (12-layer) superlattice (see Fig. 2). This is sufficient to converge the interface with respect to cell size. The relaxed interface structure is comparable to a 36-atom calculation [22]. Spin moments are initialized in VASP as 3 layers FM, 6 spin-flop [34], and 3 collinear AFM; all spins and the shuffle coordinates of interface layers are then relaxed. Figure 2 shows the lowest energy spin and shuffle configurations obtained from this starting state. In a shock transformation front, successive [001] layers would undergo spin rotation and shuffle along $[1\bar{1}0]$, and the interface would move to the right. In actuality, the ϵ and interface regions would undergo additional compression. This constrained geometry estimates the martensitic shuffle barrier inside the interface, analogous to the bulk barrier in Fig. 1, where [001] layer spacing is also held constant. It is not intended to be a faithful model of structure or dynamics at the shock front, only to expose the effect of magnetic frustration on the barrier between FM and AFM domains near the coexistence line.

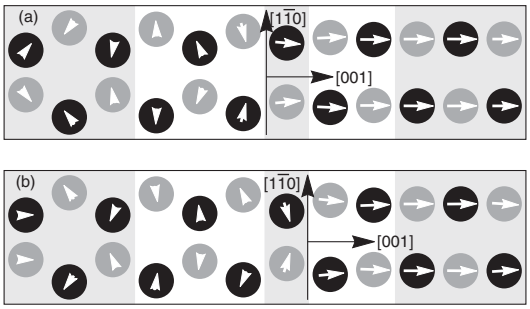

FIG. 2. Constrained model of the [001] α-ϵ interface. Black and gray circles denote alternate [110] layers of atoms; white arrows indicate local moments from VASP. [110] layers are fixed; all [001] spacings are at 8% compression. Atoms in the gray regions are fully constrained, shuffle coordinates in white regions, and all spins are relaxed. The rightmost region shows three [001] layers of untransformed, elastically strained α; three layers of fully transformed ϵ-like phase are at left. In (a), the white regions and gray band at center show a metastable interface structure. In (b), the center region shows the lowest-energy configuration; two atoms are manually displaced along $[1\bar{1}0]$ as the interface shifts right. Coordinate axes are positioned at the α-ϵ interface.

To study the transition barrier, the sixth atomic layer from the right of Fig. 2 (shaded gray) is manually displaced by different amounts, $\delta_{[6]}$ from the configurations in Fig. 2 towards bcc or hcp, while other degrees of freedom listed above are relaxed. This approximates propagating the transformation front across one layer. The total energy is recorded versus $\delta_{[6]}$, and the resulting energy barrier is shown by the black solid curve in Fig. 3. The sixth layer is structurally bistable, with local minima on both the bcc-like and hcp-like sides ($\delta \sim 0.1$ and 0.2, respectively). The martensitic barrier for this single interface layer is greatly reduced compared to the bulk value in Fig. 1.

Thermal magnetic fluctuations are expected to reduce the free energy barrier even further, as in the Monte Carlo model for the bulk. To bound the effect at the interface, the

atomic coordinates in layer 6 are held fixed and the two spins in that layer alone are constrained to rotate in spin-flop states towards collinear FM or AFM. All other degrees of freedom explored above are again relaxed. Figure 3 shows energies versus $\delta_{[6]}$ for a full range of spin-flop configurations, from FM aligned with [001] to collinear AFM along $[1\bar{1}0]$. (All curves show the best structure found by VASP. A more thorough search may lower these values.) Spin excitations of the two interface atoms on the order of 15 meV are sufficient to destabilize the bcc/FM configuration. The small $\Delta E_{\text{FM-AFM}}$ in this subspace indicates that the spin ordering temperature will be suppressed near the α-ϵ interface, especially when fluctuations are included for other spins in the multilayer interface. This suggests that the martensitic energy barrier at the α-ϵ boundary could be overcome by thermal spin fluctuations at as low as room temperature.

These results motivate the behavior already seen in α-ϵ [001] shock kinetics [9,10,13] and suggest further complexity. The coupling between structural dynamics and thermal magnetic order makes time-resolved shock experiments in oriented, single-crystal, temperature-controlled samples of particular interest. Different temperatures may give exponentially different activation lifetimes upon metastable compression beyond the equilibrium phase line. The sensitivity of the martensitic transition to local magnetic order also has implications for molecular dynamics studies. Interatomic potentials without spin dependence will miss changes in the martensitic barrier at α-ϵ interfaces because they neglect the associated magnetic domain boundary. Thus, they will either underestimate the (bulk) nucleation time for [001]-compressed α-Fe near coexistence, or overestimate thermal activation behavior for the martensitic displacement within the heterogeneous magnetic domain boundary. If martensitic displacement at the interface were thermally activated, the transformation front would still propagate by localized defect motion, but a high reacting defect density might also initiate plastic relaxation. Such behavior is not seen in experiment [9,10] or in barrier-free atomistic simulations [12].

Existing interatomic potentials give reasonable behavior at the single crystal shock transformation front, where the martensitic barrier is shown to be small. The correct transition pathway and one- or two-wave shock structure are predicted [9,10,12], and the c/a ratio [10] and hcp domain size [11] are consistent with experiment. (Reconciling this agreement with the persistent bulk martensitic barrier found here motivates the calculations for Figs. 2 and 3.) However, the adiabatic approximation made here and in deriving the MD interatomic potentials, that of partially separating the coupled magnon and phonon dynamics, is not strictly applicable given similar time scales. A complete understanding of Fe shock experiments may require an integrated spin and molecular dynamics simulation. Finally, the effects of rapid shock compression

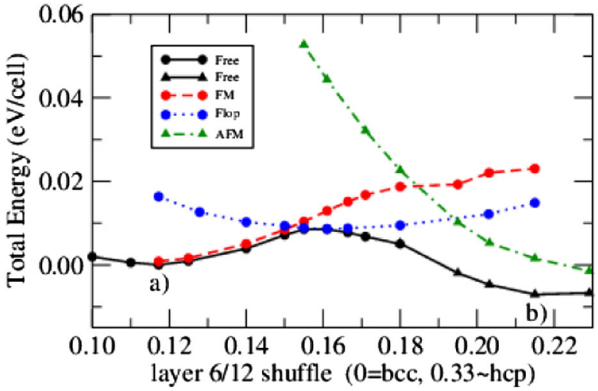

FIG. 3. Energy of the model α-ϵ interface versus $\delta_{[6]}$, coordinate of the sixth layer of the superlattice from the right in Fig. 2; here $\delta = 0$ $(1/3)$ corresponds to bcc (hcp). The energy zero corresponds to the metastable structure (a); the global energy minimum corresponds to configuration (b) in Fig. 2. The black solid curve allows all spins to relax, including a magnetic reordering in the hcp region, indicated where symbols change from circles to triangles. The blue dotted curve constrains local moments in the sixth layer to a spin-flop configuration like the relaxed transition state. The red dashed curve corresponds to FM with spins along [001] in layer 6, and the green dashed-dotted curve holds these spins antiparallel along $[1\bar{1}0]$.

on magnetization and of Faraday's law are not included in these simulations. This may suggest more complex dynamics as well as additional ways to characterize the material evolution under shock.

We provide evidence of magnetostructural coupling in uniaxially strained Fe using two approaches: (i) Monte Carlo treatment of a generalized Heisenberg model fit to bulk DFT energies, and (ii) constrained DFT calculations of an idealized α-ϵ interface. We find that thermal magnetic disorder substantively reduces the bulk martensitic transition barrier, but that it remains sizable even for large uniaxial compressions. We also establish that magnetic frustration at the α-ϵ interface reduces the barrier yet further, explaining the facile and reversible transformation between phases noted in time-resolved single shock measurements. The shock behavior of Fe may be unexpectedly sensitive to finite-temperature magnetic order. These effects are absent from existing large-scale, atomistic studies of shock transformation in Fe. Their inclusion would improve understanding of the transformation kinetics, as could experimental study of single crystal samples at different temperatures.

The authors thank Hector Lorenzana for helpful collaboration, and Jon Belof for informative discussions. We also thank Timothy Germann for providing the Fe interatomic potential in Ref. [12]. This work was supported by the Laboratory Directed Research and Development (LDRD) Program at LLNL under tracking code No. 13-ERD-044. This work was performed under the auspices of the U.S. Department of Energy by Lawrence Livermore National Laboratory under Contract DE-AC52-07NA27344.

*surh1@llnl.gov
†benedict5@llnl.gov
‡sadigh1@llnl.gov

[1] D. Bancroft, E. L. Peterson, and S. Minshall, J. Appl. Phys. **27**, 291 (1956).
[2] J. C. Jamieson and A. W. Lawson, J. Appl. Phys. **33**, 776 (1962).
[3] G. Steinle-Neumann, L. Stixrude, and R. E. Cohen, Proc. Natl. Acad. Sci. U.S.A. **101**, 33 (2004); R. Cohen and S. Mukherjee, Phys. Earth Planet. Inter. **143–144**, 445 (2004), New Developments in High-Pressure Mineral Physics and Applications to the Earth's Interior; G. Steinle-Neumann, R. E. Cohen, and L. Stixrude, J. Phys. Condens. Matter **16**, S1109 (2004).
[4] A. B. Papandrew, M. S. Lucas, R. Stevens, I. Halevy, B. Fultz, M. Y. Hu, P. Chow, R. E. Cohen, and M. Somayazulu, Phys. Rev. Lett. **97**, 087202 (2006).
[5] A. Monza, A. Meffre, F. Baudelet, J.-P. Rueff, M. d'Astuto, P. Munsch, S. Huotari, S. Lachaize, B. Chaudret, and A. Shukla, Phys. Rev. Lett. **106**, 247201 (2011).
[6] J. P. Rueff, M. Krisch, Y. Q. Cai, A. Kaprolat, M. Hanfland, M. Lorenzen, C. Masciovecchio, R. Verbeni, and F. Sette, Phys. Rev. B **60**, 14510 (1999).
[7] O. Mathon, F. Baudelet, J. P. Itié, A. Polian, M. d'Astuto, J. C. Chervin, and S. Pascarelli, Phys. Rev. Lett. **93**, 255503 (2004).
[8] V. Iota, J.-H. P. Klepeis, C.-S. Yoo, J. Lang, D. Haskel, and G. Srajer, Appl. Phys. Lett. **90**, 042505 (2007).
[9] D. H. Kalantar, J. F. Belak, G. W. Collins, J. D. Colvin, H. M. Davies, J. H. Eggert, T. C. Germann, J. Hawreliak, B. L. Holian, K. Kadau, P. S. Lomdahl, H. E. Lorenzana, M. A. Meyers, K. Rosolankova, M. S. Schneider, J. Sheppard, J. S. Stölken, and J. S. Wark, Phys. Rev. Lett. **95**, 075502 (2005).
[10] J. A. Hawreliak, B. El-Dasher, H. Lorenzana, G. Kimminau, A. Higginbotham, B. Nagler, S. M. Vinko, W. J. Murphy, T. Whitcher, J. S. Wark, S. Rothman, and N. Park, Phys. Rev. B **83**, 144114 (2011); J. Hawreliak, J. D. Colvin, J. H. Eggert, D. H. Kalantar, H. E. Lorenzana, J. S. Stölken, H. M. Davies, T. C. Germann, B. L. Holian, K. Kadau, P. S. Lomdahl, A. Higginbotham, K. Rosolankova, J. Sheppard, and J. S. Wark, Phys. Rev. B **74**, 184107 (2006).
[11] J. A. Hawreliak, D. H. Kalantar, J. S. Stölken, B. A. Remington, H. E. Lorenzana, and J. S. Wark, Phys. Rev. B **78**, 220101 (2008).
[12] K. Kadau, T. C. Germann, P. S. Lomdahl, and B. L. Holian, Science **296**, 1681 (2002); Phys. Rev. B **72**, 064120 (2005); K. Kadau, T. C. Germann, P. S. Lomdahl, R. C. Albers, J. S. Wark, A. Higginbotham, and B. L. Holian, Phys. Rev. Lett. **98**, 135701 (2007).
[13] J. C. Crowhurst, B. W. Reed, M. R. Armstrong, H. B. Radousky, J. A. Carter, D. C. Swift, J. M. Zaug, R. W. Minich, N. E. Teslich, and M. Kumar, J. Appl. Phys. **115**, 113506 (2014).
[14] M. Ekman, B. Sadigh, K. Einarsdotter, and P. Blaha, Phys. Rev. B **58**, 5296 (1998).
[15] K. J. Caspersen, A. Lew, M. Ortiz, and E. A. Carter, Phys. Rev. Lett. **93**, 115501 (2004).
[16] R. Lizárraga, L. Nordström, O. Eriksson, and J. Wills, Phys. Rev. B **78**, 064410 (2008).
[17] This transformation to hcp is incomplete because the c/a ratio that results is $\sqrt{3}$ instead of the ideal $\sqrt{8}/3$.
[18] G. Kresse and J. Furthmüller, Phys. Rev. B **54**, 11169 (1996).
[19] J. P. Perdew, K. Burke, and M. Ernzerhof, Phys. Rev. Lett. **77**, 3865 (1996); **78**, 1396 (1997).
[20] G. Kresse and D. Joubert, Phys. Rev. B **59**, 1758 (1999).
[21] D. Hobbs, G. Kresse, and J. Hafner, Phys. Rev. B **62**, 11556 (2000).
[22] See Supplemental Material http://link.aps.org/supplemental/10.1103/PhysRevLett.117.085701 for details the generalized Heisenberg Hamiltonian and its sampling by classical Metropolis Monte Carlo methods and includes an investigation of finite size effects on the schematic DFT model for the α-ε interface., which includes Refs. [23,24].
[23] K. Huang, *Statistical Mechanics*, 2nd ed. (Wiley, New York, 1987).
[24] S. Kirkpatrick, C. D. Gelatt, and M. P. Vecchi, Science **220**, 671 (1983).
[25] C. Kittel, *Introduction to Solid State Physics*, 5th ed. (John Wiley & Sons, Inc., New York, 1976), p. 31.
[26] S. K. Satija, R. P. Comès, and G. Shirane, Phys. Rev. B **32**, 3309 (1985).
[27] H. Hasegawa, M. W. Finnis, and D. G. Pettifor, J. Phys. F **15**, 19 (1985).
[28] S. Mankovsky, S. Polesya, H. Ebert, W. Bensch, O. Mathon, S. Pascarelli, and J. Minár, Phys. Rev. B **88**, 184108 (2013).
[29] N. M. Rosengaard and B. Johansson, Phys. Rev. B **55**, 14975 (1997).
[30] R. Singer, F. Dietermann, and M. Fähnle, Phys. Rev. Lett. **107**, 017204 (2011).
[31] C. Kittel, *Introduction to Solid State Physics*, 5th ed. (John Wiley & Sons, Inc., New York, 1976), p. 455.
[32] N. Metropolis, A. W. Rosenbluth, M. N. Rosenbluth, A. H. Teller, and E. Teller, J. Chem. Phys. **21**, 1087 (1953).
[33] J. C. Boettger and D. C. Wallace, Phys. Rev. B **55**, 2840 (1997).
[34] D. Spišák and J. Hafner, Surf. Sci. **601**, 4348 (2007); eCOSS-24, edited by J. Jupille and P. Dumas, *Proceedings of the 24th European Conference on Surface Science*, Vol. 601.